Substrate Doping Concentration Dependence of Electron Mobility Enhancement in Uniaxial Strained (110)/<110> nMOSFETs

Wookyung Sun, Sujin Choi, and Hyungsoon Shin

Abstract—**The substrate doping concentration dependence of strain-enhanced electron mobility in (110)/<110> nMOSFETs is investigated by using a self-consistent Schrödinger-Poisson solver. The electron mobility model includes Coulomb, phonon, and surface roughness scattering. The calculated results show that, in contrast to (100)/<110> case, the longitudinal tensile strain-induced electron mobility enhancement on the (110)/<110> can be increased at high substrate doping concentration.**

Index Terms—**Electron mobility, stress, strain, intravalley phonon mobility, intervalley phonon mobility, wafer orientation**

I. INTRODUCTION

As CMOS technology has become more advanced, various types of 3-D multigate structures such as double-gate (DG) FinFETs and tri-gate MOSFETs or mobility enhancement technology using strain have been studied [1-3]. The fin structure is useful to implement the double-gate structure and then the electron mobility characteristic of <110> current direction on (110) wafer orientation is important because (110)/<110> became the channel of DG FinFETs at a conventional (100) wafer orientation. Moreover, as the device dimension shrinks, it is necessary to enhance the carrier mobility of DG FinFETs by strain because the strain changes the electronic band structure resulting in the change of carrier mobility [4-8].

In our previous work, we suggested that low substrate doping concentration on the (100)/<110> nMOSFETs is more helpful for strain-induced electron mobility enhancement at high effective electric field [9]. However, there is very little information on the understanding of substrate doping concentration (N_{sub}) dependence of electron mobility enhancement induced by uniaxial strain on (110)/<110>.

This paper is organized as follows. Section II presents the models for electron mobility and stress effects. In Section III, the results of our simulation are presented and analyzed, and Section IV reports the discussions and conclusions.

II. MOBILITY SIMULATION

In a semiconductor, there are different scattering mechanisms such as Coulomb scattering, phonon scattering and surface roughness scattering. These scattering events influence the mobility of carrier and the carrier mobility is given by

$$\mu = \frac{q \cdot \tau}{m^*}, \tag{1}$$

where τ is the momentum-relaxation time and m^* is the conductivity effective mass of carrier [2]. When multiple scattering mechanisms occur, the total carrier mobility is typically obtained by Matthiessen's rule. However, it has been known that the Matthiessen rule is not exact and it

Manuscript received May. 1, 2014; accepted Jul. 27, 2014
A part of this work was presented in Korean Conference on Semiconductors, Seoul in Korea, Feb. 2014.
Department of Electronic Engineering, Ewha Womans University
E-mail : hsshin@ewha.ac.kr

results in large inaccuracies in the mobility extraction [6-8]. To calculate the total mobility more exactly, we used Momentum Relaxation Time (MRT) method. When different scattering mechanisms are included in the calculations, the total MRT is obtained by summing the inverse of the MRTs and it can be expressed as

$$\frac{1}{\tau^{(i)}(E)} = \sum_{s} \frac{1}{\tau_s^{(i)}(E)}, \tag{2}$$

where $\tau_s^{(i)}(E)$ is the MRT due to the scattering mechanism '*s*' alone and index *i* is the subband [8]. To consider the total mobility, we take into account the Coulomb scattering (τ_{coul}), intravalley phonon scattering (τ_{intra}), intervalley phonon scattering (τ_{inter}), and surface roughness scattering (τ_{sr}) MRTs. The total relaxation rate ($1/\tau$), the electron mobility in the *i* th subband (μ_i), and total electron mobility (μ_{total}) are given by [10, 11]

$$\frac{1}{\tau^i} = \frac{1}{\tau^i_{Coulomb}} + \frac{1}{\tau^i_{intra}} + \frac{1}{\tau^i_{inter}} + \frac{1}{\tau^i_{surface}}, \tag{3}$$

$$\mu^i = \frac{q\int_{E_i}^{\infty}(E-E_i)\,\tau^i(-\partial f/\partial E)dE}{m_{c,i}\int_{E_i}^{\infty}(E-E_i)\,(-\partial f/\partial E)dE}, \tag{4}$$

$$\mu_{total} = \frac{\sum_i \left(\mu^i N_i\right)}{N_S}, \tag{5}$$

where $m_{c,i}$ is the conductivity mass of *i* th subband. N_i is the carrier density of the *i* th subband, and N_s is the total carrier density.

The momentum-relaxation rate of Coulomb scattering is given by [12]

$$\frac{1}{\tau_{Coulomb}} = \frac{N_I q^4\left[\ln\left(1+\gamma^2\right) - \frac{\gamma^2}{1+\gamma^2}\right]}{16\sqrt{2m_c}\,\pi\varepsilon_{si}^{\,2}\varepsilon_0^{\,2}E^{3/2}}, \tag{6}$$

$$\gamma^2 = \frac{8m_c L_D^{\,2}E}{\hbar^2},$$

where N_I is the impurity concentration, ε_0 is the permittivity of free space, ε_{si} is the relative permittivity of Si, and L_D is the Debye length.

The momentum relaxation rate by intravalley acoustic phonons ($1/\tau^i_{intra}$) and intervalley optical phonons ($1/\tau^i_{inter}$) scattering from the *i* th subband to the *j* th subband is given by [11]

$$\frac{1}{\tau^i_{intra}(E)} = \sum_j \frac{n_i^{ac} m_{d,j} D^2_{ac,eff} k_B T}{\hbar^3 \rho s_l^2} F_{i,j} U(E-E_j), \tag{7}$$

$$\frac{1}{\tau^i_{inter}(E)} = \sum_j \left\{ \sum_k^{\{f,g\}} \frac{n_{ij}^{f,g} m_{d,j} D^2_{k,eff}}{\hbar\rho E_k} F_{i,j}\left(N_k + \frac{1}{2} \pm \frac{1}{2}\right) \cdot \frac{1-f(E\mp E_k)}{1-f(E)} U(E\mp E_k - E_j)\right\}, \tag{8}$$

$$F_{i,j} = \int_{-\infty}^{+\infty} \left|\xi_i(z)\right|^2 \left|\xi_j(z)\right|^2 dz, \tag{9}$$

where *U(x)* is the Heaviside step function, *k* is the index of phonons, E_k is the energy of the *k* th intervalley phonon, N_k is the Bose-Einstein distribution function, and *f(E)* is the Fermi-Dirac distribution function. The physical parameters used in equations are listed in Table 1. In (8), *f* and *g* are the types of intervalley scattering and $F_{i,j}$ is the form factor determined by the wave functions of the *i* th and the *j* th subbands. In order to more accurately calculate the phonon scattering rate, we use the concept of effective deformation potential which means the deformation potential is changed by effective electric field (E_{eff}) [13]. $D_{ac,eff}$ is the effective intravalley deformation potential for acoustic phonon scattering. $D_{k,eff}$ is the effective deformation potential of the *k* th intervalley phonon.

The traditional theory of interface roughness scattering has already been developed and expressions for that are given by [14, 15]

$$\frac{1}{\tau_{surface}} = \frac{\pi m_d \left[\Delta\Lambda q E_{eff}\right]^2}{\hbar^3}, \tag{10}$$

where Δ is the root-mean-square height of interface roughness and Λ is the lateral decay length of interface roughness.

Analytical expressions for the strain-induced valley splitting and effective mass changes of the (110)/<110> have been reported in [16]

$$\begin{aligned} E_{\Delta 2,0} &= \Xi_d(\varepsilon_{xx}+\varepsilon_{yy}+\varepsilon_{zz}) + \Xi_u\varepsilon_{zz} + E^{shear}_{\Delta z,0} \\ &= 74.97T_W - 17.28(T_L+T_V) - 3.62(-T_L+T_V)^2, \end{aligned} \tag{11}$$

Table 1. Physical parameters used in this paper

Symbol	Value	Definition
m_0	9.11×10^{-31} kg	free electron mass
ρ	2329 kg/m^3	crystal mass density
s_l	9037 m/s	longitudinal sound velocity
Δ	3.5 nm	root-mean-square height of interface roughness
Λ	8 nm	lateral decay length of interface roughness
$m_{c\,\Delta2}$	0.19 m_0	conductivity mass of Δ2
$m_{c\,\Delta4}$	0.553 m_0	conductivity mass of Δ4
$m_{d\,\Delta2}$	0.417 m_0	density of state mass of Δ2
$m_{d\,\Delta4}$	0.324 m_0	density of state mass of Δ4
$m_{z\,\Delta2}$	0.19 m_0	quantization mass of Δ2 (parabolic)
$m_{z\,\Delta4}$	0.315 m_0	quantization mass of Δ4
D_{ac}	12 eV	intravalley deformation potential at $E_{\text{eff}} = 0.1$ MV/cm
D_k	8×10^8 eV/cm	intervalley deformation potential at $E_{\text{eff}} = 0.1$ MV/cm
E_k	59 meV 63 meV	energy of *f* type intervalley energy of *g* type intervalley
$n_{\Delta2}^{ac}$ $n_{\Delta4}^{ac}$	1 1	degeneracy number of each valley for intravalley scattering
$n^g_{\Delta2\,\Delta2}$ $n^f_{\Delta2\,\Delta4}$ $n^g_{\Delta4\,\Delta4}$ $n^f_{\Delta4\,\Delta2}$ $n^f_{\Delta4\,\Delta4}$	1 4 1 2 2	degeneracy number of each valley for intervalley scattering
m_l	0.916 m_0	longitudinal effective mass
m_t	0.19 m_0	transverse effective mass
Ξ_u	9.29 eV	uniaxial deformation potential
Ξ_d	1.1 eV	dilatation deformation potential
Θ	0.53 eV	k·p model parameter
η	-0.809	
k	0.0189	

$$
\begin{aligned}
E_{\Delta4,0} &= \Xi_d(\varepsilon_{xx}+\varepsilon_{yy}+\varepsilon_{zz})+\Xi_u\varepsilon_{xx} \\
&= \Xi_d(\varepsilon_{xx}+\varepsilon_{yy}+\varepsilon_{zz})+\Xi_u\varepsilon_{yy} \\
&= 28.85(T_L+T_V)-17.28T_W,
\end{aligned} \tag{12}
$$

where $E_{\Delta2,0}$ and $E_{\Delta4,0}$ are the strain induced energy shifts for Δ2 and Δ4 valley, respectively. T_L, T_W, and T_V are the stress components in the gate length, gate width, and gate vertical direction with gigapascal scale, respectively. The masses of Δ2 valley are changed by the shear strain, and they are given by [16, 17]

$$
\begin{aligned}
m_{\Delta2,c} &= m_t\left(1-|\eta|\frac{S_{44}}{4k}(-T_L+T_V)\right)^{-1}, \\
m_{\Delta2,q} &= m_{q,eff}\left(1-\frac{S_{44}^{\,2}}{16k^2}(-T_L+T_V)^2\right)^{-1}, \\
m_{\Delta2,d} &= \sqrt{m_l\cdot m_t}\left(1+|\eta|\frac{S_{44}}{4k}(-T_L+T_V)\right)^{-1},
\end{aligned} \tag{13}
$$

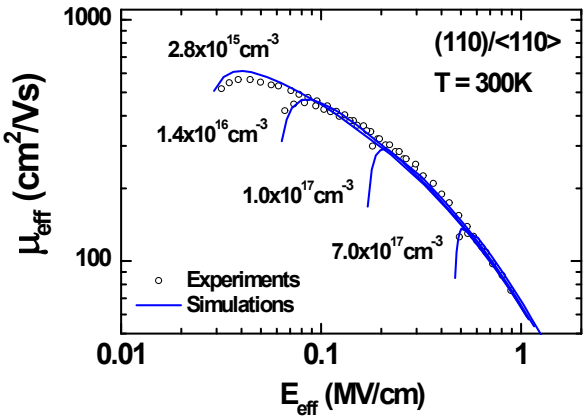

Fig. 1. E_{eff} dependence of the electron mobility for various N_{sub}. The symbols represent the experimental data from [18]. The solid lines represent the numerically calculated μ_{eff}.

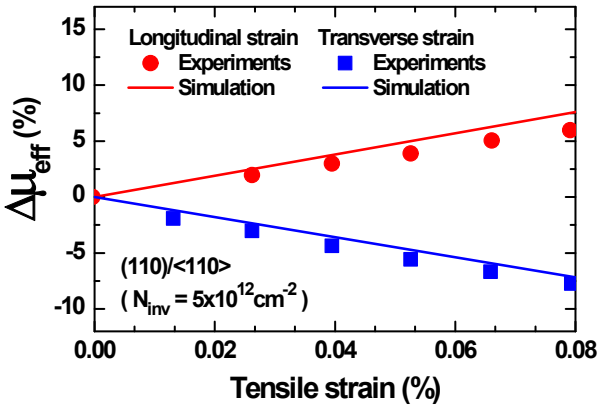

Fig. 2. Strain dependence of the μ_{eff} enhancement induced by uniaxial longitudinal and transverse tensile strain. The symbols represent the experimental data from [19]. The solid lines represent numerically calculated mobility enhancement.

where $m_{\Delta2,c}$, $m_{\Delta2,q}$, and $m_{\Delta2,d}$ are the conductivity, quantization, and density of state mass of Δ2 valley, respectively. The physical parameters used in (13) are listed in Table 1.

In Fig. 1, the calculated electron mobility in the (110)/<110> is compared with the experimental data for various N_{sub} reported in [18]. As can be seen, our calculation results show good agreement with the experimental data in all range. Fig. 2 is the strain dependence of μ_{eff} enhancement induced by uniaxial longitudinal and transverse tensile stress on (110)/<110>, and our numerically calculated results agree well with experimental data [19].

In case of (110) orientation, it is well known that E-k along <110> is non-parabolic particularly at energies greater than 0.1 eV and this non-parabolic characteristic

of (110)/<110> increases the quantization mass of Δ2 valley [16, 19]. Thus, it is important to accurately determine the subband structures in (110) nMOSFETs. To analytically describe this non-parabolic characteristic, we calculate quantization mass of Δ2 valley as [20]

$$m_{q,eff} = m_t \left(1+1.5\times\left(E_i - E_{C,s}\right)\right), \qquad (14)$$

where m_t is parabolic quantization mass of Δ2 valley, E_i is the quantization band energy, and $E_{C,s}$ is the conduction band energy at Si/SiO_2 interface. Fig. 3 is the calculated relative occupancy of the (110)/<110> inversion layer with non-parabolic energy band as a function of N_{inv} and our numerically calculated results show good agreement with reference data taken from [19]. As shown in Figs. 1-3, our numerically calculated mobility shows good agreement with the experimental data. Therefore, it is reasonable that we use our numerically calculated results to predict the strain-induced mobility enhancement for various cases.

III. Substrate Doping Dependence of Strain-induced Electron Mobility Enhancement

Fig. 4 shows the relative enhancement ratio of mobility by 0.5% uniaxial longitudinal tensile strain with several N_{sub} on (100)/<110> and it has been detailed in our previous work [9]. Fig. 5 is the relative enhancement ratio of mobility on (110)/<110> under the same condition as those used in Fig. 4 and the characteristic of (110)/<110> is quite distinct from that of (100)/<110>. In contrast to the (100)/<110>, the relative mobility enhancement ratio of (110)/<110> is larger for high N_{sub}, even if the absolute mobility of the high N_{sub} is smaller than that of the low N_{sub}. To examine the effect of N_{sub}, we compared m_c, the momentum relaxation rate by phonon scattering ($1/\tau_{ph}$), and relative occupancy with a low N_{sub} (=1.4x10^{16} cm^{-3}) and high N_{sub} (=7.0x10^{17} cm^{-3}). As a results, we found that strain-induced m_c, $1/\tau_{intra}$, and $1/\tau_{inter}$ are barely unchanged whether N_{sub} is low or high. Fig. 6 shows the change of $1/\tau_{intra}$ induced by 0.5 % uniaxial longitudinal tensile strain in high N_{sub} and low N_{sub}. As shown, the strain induces very small change in $1/\tau_{intra}$ of Δ2 valley. Not only $1/\tau_{intra}$ but also $1/\tau_{inter}$ and m_c

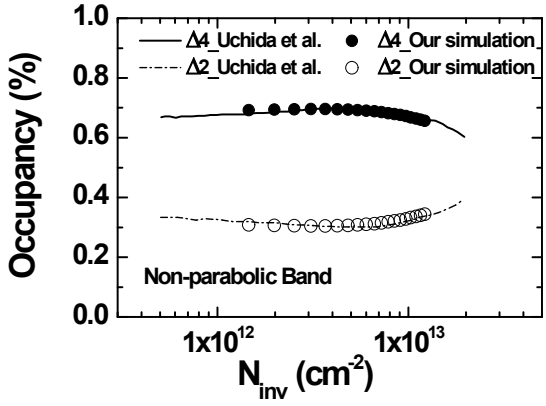

Fig. 3. The calculated relative occupancy of the (110)/<110> inversion layer with non-parabolic energy band as a function of N_{inv}. The solid lines represent the reference data taken from [19] and the symbols represent our non-parabolic simulation results.

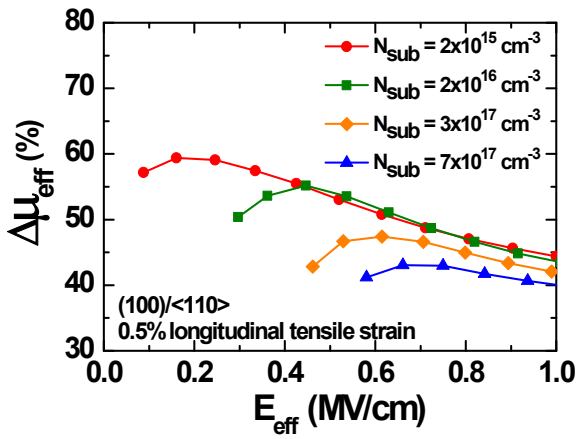

Fig. 4. Strain-induced relative mobility enhancement ratio of the (100)/<110> inversion layer as a function of E_{eff} for several N_{sub}.

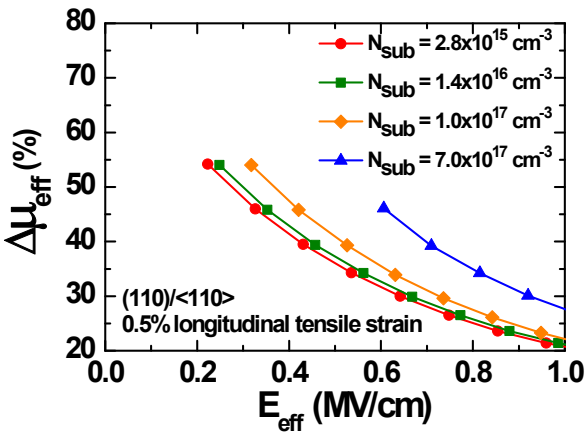

Fig. 5. Strain-induced relative mobility enhancement ratio of the (110)/<110> inversion layer as a function of E_{eff} for several N_{sub}.

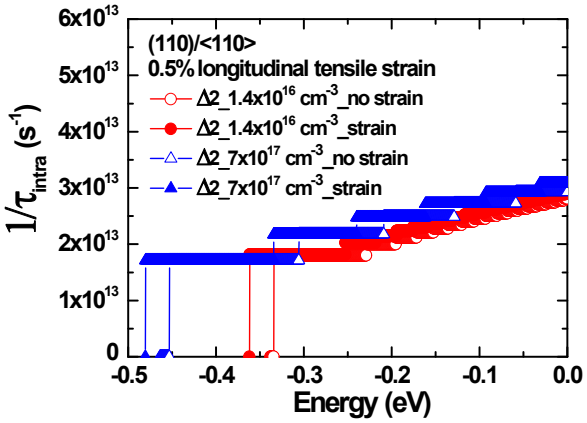

Fig. 6. Calculated momentum relaxation time of bottom energy subband for intra phonon scattering under 0.5 % longitudinal tensile strain as a function of energy in N_{sub} = 1.4×10^{16} cm^{-3} and 7×10^{17} cm^{-3}.

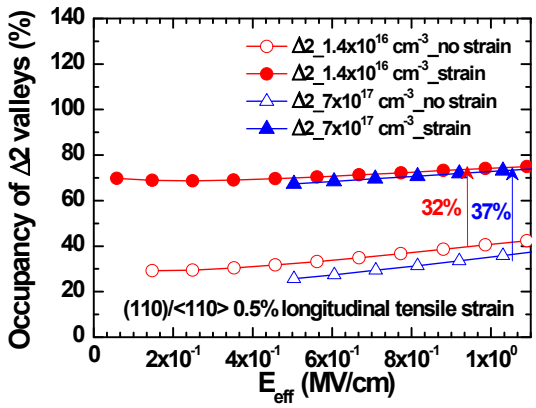

Fig. 7. Calculated Δ2 valleys relative occupancy of the (110)/<110> inversion layer as a function of E_{eff} in N_{sub} = 1.4×10^{16} cm^{-3} and 7×10^{17} cm^{-3}.

have small influence on relative electron mobility enhancement (data not shown here). Thus, intravalley, intervalley phonon scattering, and m_c are not main causes of relative mobility enhancement. However, the change of relative occupancy induced by strain is different with N_{sub}. Fig. 7 shows the calculated relative occupancy of Δ2 valleys as a function of E_{eff}. The longitudinal tensile strain enhances the population of Δ2 valleys, and the occupancy of Δ2 valleys increases by 37 % with high N_{sub} while it increases only by 32 % with low N_{sub} at E_{eff} = 1 MV/cm. It is worthy of notice that the occupancy of Δ2 valleys is higher than the occupancy of Δ4 valleys by strain and conductivity mass of Δ4 valley is about 3 times heavier than that of Δ2 valley in case of the (110)/<110>.

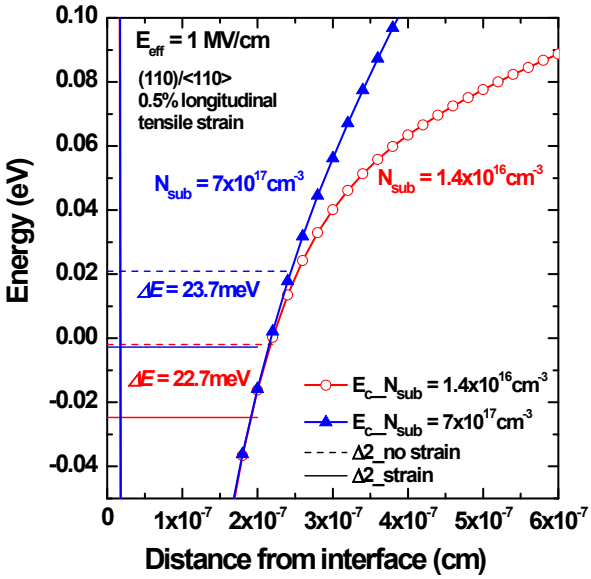

Fig. 8. Calculated E_c and bottom subband energy of Δ2 valley in N_{sub} = 1.4×10^{16} cm^{-3} and 7×10^{17} cm^{-3}. ΔE represents the energy shift of Δ2 valley induced by 0.5 % longitudinal tensile strain.

Accordingly, relative occupancy of subband is the primary reason for N_{sub} dependency on the (110)/<110>. To investigate the reason of relative occupancy change, we calculate bottom subband energy of Δ2 valley, as shown in Fig. 8. It shows the decrease of bottom subband energy of Δ2 valley in high N_{sub} is larger than that in low N_{sub} for the (110)/<110>. In conclusion, among several parameters which have an influence on mobility, the occupancy of subband is the most important parameter for stress-induced relative mobility enhancement.

IV. CONCLUSIONS

We investigated the substrate doping concentration dependence of longitudinal tensile strain-enhanced electron mobility in (110)/<110> nMOSFETs. The strain-induced electron mobility enhancement on the (110)/<110> can be increased at high substrate doping concentration and relative occupancy of sub-valleys is the major factor to determine the electron mobility enhancement. The results of this paper should be helpful in understanding the strain-induced electron mobility characteristic and advantageous for strain-induced high electron mobility.

ACKNOWLEDGMENTS

This research was supported by the National Research Foundation of Korea (NRF) funded by the Ministry of Science, ICT and Future Planning (No. 2014R1A2A2A01002219).

REFERENCES

[1] C. W. Liu, S. Maikap, and C. Y. Yu "Mobility-Enhancement Technologies," *IEEE Circuits & Device magazine*, pp. 18–23, May/Jun. 2005.

[2] N. Mohta and S. E. Thompson "Mobility enhancement," *IEEE Circuits & Device magazine*, pp. 21–36, Sep./Oct. 2005.

[3] Y. Song, H. Zhou, Q. Xu, J. Luo, H. Yin, J. Yan, and H. Zhong "Mobility Enhancement Technology for Scaling of CMOS Devices: Overview and Status," *Journal of electronic materials*, vol. 40, no. 7, pp. 1584–1612, 2011.

[4] M. V. Fischetti, F. Gámiz, and W. Hänsch, "On the enhanced electron mobility in strained-silicon inversion layers," *J. Appl. Phys.*, vol. 92, no. 12, pp. 7320–7324, Dec. 2002.

[5] S. E. Thompson, M. Armstrong, C. Auth, S. Cea, R. Chau, G. Glass, T. Hoffman, J. Klaus, Z. Ma, B. Mcintyre, A. Murthy, B. Obradovic, L. Shifren, S. Sivakumar, S. Tyagi, T. Ghani, K. Mistry, M. Bohr, and Y. El-Mansy, "A logic nanotechnology featuring strained-silicon," *IEEE Electron Device Lett.*, vol. 25, no. 4, pp. 191–193, Apr. 2004.

[6] K. W. Ang, K. J. Chui, C. H. Tung, N. Balasubramanian, M. Fu. Li, G. S. Samudra, and Y. C. Yeo, "Enhanced strain effects in 25-nm gate-length thin-body nMOSFETs with silicon-carbon source/drain and tensile-stress liner," *IEEE Electron Device Lett.*, vol. 28, no. 4, pp. 301–304, Apr. 2007.

[7] K. Uchida, M. Saitoh, and S. Kobayashi, "Carrier transport and stress engineering in advanced nanoscale transistors from (100) and (110) transistors to carbon nanotube FETs and beyond," in *IEDM Tech. Dig.,* 2008, pp. 1–4.

[8] S. Takagi, T. Irisawa, T. Tezuka, T. Numata, S. Nakaharai, N. Hirashita, Y. Moriyama, K. Usuda, E. Toyoda, S. Dissanayake, M. Shichijo, R. Nakane, S. Sugahara, M. Takenaka, and N. Sugiyama, "Carrier-transport-enhanced channel CMOS for improved power consumption and performance," *IEEE Trans. Electron Devices*, vol. 55, no. 1, pp. 21–39, Jan. 2008.

[9] W. Sun and H. Shin, "Substrate doping concentration dependence of electron mobility using the effective deformation potential in uniaxial strained nMOSFETs," in *TENCON,* 2013, pp. 166–167.

[10] D. Esseni and F. Driussi, " A Quantitative error analysis of the mobility extraction according to the matthiessen rule in advanced MOS transistors," *IEEE Trans. on Elec. Dev.*, vol. 58, no. 8, pp. 2415-2422, 2011.

[11] S. Takagi, J. L. Hoyt, J. J. Welser, and J. F. Gibbons, "Comparative study of phonon-limited mobility of two-dimensional electrons in strained and unstrained Si metal-oxide-semiconductor field-effect transistors," *J. Appl. Phys.*, vol. 80, no. 3, pp. 1567–1577, Aug. 1996

[12] M. Lundstrom, *Fundamentals of carrier transport,* second ed., Cambridge, New York, 2000, pp.70.

[13] W. Sun and H. Shin, "Optimization of uniaxial stress for high electron mobility on biaxially-strained n-MOSFETs," *Solid-State Electronics*, vol. 94, pp.23-27, Apr. 2014.

[14] T. Ando, A. B. Fowler, and F. Stern, "Electronic properties of two-dimensional systems," *Rev. Mod. Phys.*, vol 54 (1982) pp. 437-672, 1982.

[15] K. Masaki, C. Hamaguchi, K. Taniguchi, and M. Iwase, "Electron mobility in Si inversion layers," *Japan. J. Appl. Phys.*, vol. 28, no. 10, pp. 1856–1863, Oct. 1989.

[16] N. Serra, and D. Esseni, "Mobility enhancement in strained n-FinFETs: Basic insight and stress engineering," *IEEE Trans. Electron Devices*, vol. 57, no. 2, pp. 482–490, Feb. 2010.

[17] E. Ungersboeck, S. Dhar, G. Karlowatz, V. Sverdlov, H. Kosina, and S. Selberherr, "The effect of general strain on the band structure and electron mobility of silicon," *IEEE Trans. Electron Devices*, vol. 54, no. 9, pp. 2183–2190, Sep. 2007.

[18] S. Takagi, A. Toriumi, M. Iwase, and H. Tango, "On the universality of inversionlayer mobility in Si MOSFET's: Part II – Effects of surface orientation," *IEEE Trans. Electron Devices*, vol. 41,

no. 12, pp. 2363–2368, Dec. 1994.

[19] K. Uchida, A. Kinoshita, and M. Saitoh, "Carrier transport in (110) nMOSFETs : Subband structures, non-parabolicity, mobility characteristics, and uniaxial stress engineering," in *IEDM Tech. Dig.,* 2006, pp. 1–4.

[20] J. Wang, A. Rahman, A. Ghosh, G. Klimeck, and M. Lundstrom, "On the validity of the parabolic effective-mass approximation for the I-V calculation of silicon nanowire transistors," *IEEE Trans. Electron Devices*, vol. 52, no. 7, pp. 1589–1594, Jul. 2005.

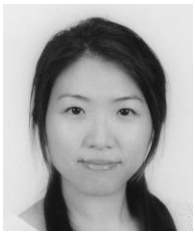

Wookyung Sun received the B.S. and M.S. degrees in electronics engineering from Ewha Womans University, Seoul, Korea, in 1999 and 2001, respectively. From 2001 to 2009, she was with Hynix semiconductor, Ltd., in Korea, where she was engaged in research on the development of DRAM memory. She is currently working toward the Ph.D. degree in electronics engineering from Ewha Womans University, Seoul, Korea. Her research interest includes the 3-D multi gate devices, strain effect based on Si MOSFETs, and TFT devices.

Sujin Choi received the B.S. degree in electronics engineering from Ewha Womans University, Seoul, Korea, in 2013. She is currently working toward the Integrated Ph.D. degree in electronics engineering from Ewha Womans University, Seoul, Korea. Her research interest includes the 3-D multi gate devices, strain effect based on Si MOSFETs and 3-D multi gate devices.

Hyungsoon Shin received the B.S. degree in electronics engineering from Seoul National University, Seoul, Korea, in 1982, and the M.S. and Ph.D. degrees in electrical engineering from the University of Texas at Austin, Austin, in 1984 and 1990, respectively. From 1990 to 1994, he was with LG Semicon Company, Ltd., in Korea, where he was engaged in research on the development of DRAM, SRAM, and Flash memory. Since 1995, he has been with the Department of Electronics Engineering, EWHA Womans University, Seoul. His current research interests include new processes, devices, and circuit developments and modeling based on Si, both for high-density memory and RF ICs.